DISTURBED STRESS FIELD MODEL FOR REINFORCED CONCRETE: VALIDATION

By F. J. Vecchio,[1] D. Lai,[2] W. Shim,[3] and J. Ng[4]

ABSTRACT: The results of analytical investigations are presented supporting the disturbed stress field model as a viable conceptual model for describing the behavior of cracked reinforced concrete elements. The theory is shown to be phenomenologically more correct, relative to typical fixed-crack or rotating-crack models, in its representation of the rotation of stress and strain fields in cracked concrete. The inclusion of rigid slip along crack surfaces allows for a divergence between principal stress and principal strain directions in the concrete, with the rotation of stresses and crack directions shown to typically lag behind that of strains. This behavior is found to be consistent with experimentally observed response. Corroboration with data from beam, panel, and shear wall test specimens shows the theory to accurately model response over a wide range of conditions. In general, results are improved relative to those obtained from the modified compression field theory. Current deficiencies in the theory are identified, and possible future work is discussed.

INTRODUCTION

The disturbed stress field model (DSFM) was recently proposed as an alternative model for representing the behavior of cracked reinforced concrete elements. It is a smeared rotating crack model that explicitly allows for rigid slip along crack interfaces in its development of compatibility, equilibrium, and constitutive relations. The inclusion of crack slip results in a "delayed" rotation of cracks; that is, where the rotation of the principal stress directions typically lags behind the rotation of the principal strains. As such, the theory occupies a middle ground between full rotating-crack models and fixed-crack models. Various alternative approaches are possible for representing crack slip deformations, including explicit crack shear stress-slip relations, fixed lag-angle relationships, and hybrid formulations combining the two. Full details regarding the theoretical formulation, and its implementation into nonlinear finite-element procedures, were provided previously in the literature (Vecchio 2000, 2001).

The predecessor of the DSFM is the modified compression field theory (MCFT), developed by Vecchio and Collins (1982) some 20 years ago and essentially unchanged since. The MCFT is a full rotating-crack model built around constitutive relations derived from extensive experimental investigations. As previously discussed, the MCFT provides good accuracy in the modeling of cracked reinforced concrete structures over a wide range of conditions. However, under some outlying conditions, the MCFT has shown to suffer from reduced accuracy.

Relative to the MCFT, the DSFM attempts to provide a better phenomenological representation of the behavior of concrete by explicitly allowing for crack shear slip in the description of element deformation. It dispenses with the condition that principal stress and principal strain directions in the concrete remain coincident and removes a crack shear check that proved troublesome in readings of the MCFT by others. Furthermore, in representing the softening of cracked concrete in compression, it reduces the influence ascribable to transverse cracking strains to a level comparable to that reported by other researchers (Vecchio 2001).

In support of the theoretical formulations, this paper provides further insight into the behavior mechanisms implicit in the proposed model. Corroboration of the model's accuracy is also provided by examining data from several series of test specimens demonstrating improved breadth in accuracy relative to the MCFT.

GENERAL BEHAVIOR

To identify some important behavior tendencies and to show how they are represented in the proposed formulation, consider Panel PV10 tested by Vecchio and Collins (1986). This panel was orthogonally reinforced (ρ_x = 1.8%, ρ_y = 1.0%) and subjected to monotonic pure shear. Shown in Fig. 1 are photographs of the test panel at various stages of loading; note that the reinforcement directions, and hence the reference x,y-axes, are aligned with the panel edges. Given in Fig. 2 are the corresponding load-deformation plots obtained from test data. Figs. 2(a and b) show the measured strains in the longitudinal (x) and transverse (y) reinforcement directions. Fig. 2(c) gives the measured (apparent) normal shear strain response, and Fig. 2(d) shows the calculated inclinations of the stress (θ_σ) and strain (θ_ε) fields.

At a load of v = 3.5 MPa [load stage 5; Fig. 1(a)], the transverse reinforcement is on the verge of yielding. The inclination of the strain field at this point has increased to about 50°, as determined directly from strain measurements on the panel. The inclination of the stress field, also determined from the test data, essentially remains at 45°. This is significant when coupled with the observation that, as seen in Fig. 1(a), the inclination of the cracks shows no apparent deviation from 45° relative to the x-axis. At a load of v = 3.97 MPa [load stage 7; Fig. 1(b)], the panel reaches its ultimate load capacity, and the transverse reinforcement is well into yielding. The inclination of the measured principal strains has increased to 55°, while the orientation of the principal stresses has begun to change and is at approximately 47°. In Fig. 1(b), a slight reorientation of the crack direction is becoming discernible. Figs. 1(c and d) show the accelerated reorientation of cracks during postpeak response and the final failure stage. This gradual rotation of crack direction was observed, in general, to be more pronounced in elements containing lesser amounts of transverse reinforcement relative to the amounts of longitudinal reinforcement present.

Observations that can be drawn from the observed behavior-

[1]Prof., Dept. of Civ. Engrg., Univ. of Toronto, Toronto, Canada M5S 1A4.

[2]Grad. Student, Dept. of Civ. Engrg., Univ. of Toronto, Toronto, Canada M5S 1A4.

[3]Grad. Student, Dept. of Civ. Engrg., Univ. of Toronto, Toronto, Canada M5S 1A4.

[4]Student, Dept. of Civ. Engrg., Univ. of Toronto, Toronto, Canada M5S 1A4.

Note. Associate Editor: Julio Ramirez. Discussion open until September 1, 2001. To extend the closing date one month, a written request must be filed with the ASCE Manager of Journals. The manuscript for this paper was submitted for review and possible publication on January 7, 2000; revised October 25, 2000. This paper is part of the ***Journal of Structural Engineering***, Vol. 127, No. 4, April, 2001. ©ASCE, ISSN 0733-9445/01/0004-0350–0358/$8.00 + $.50 per page. Paper No. 22220.

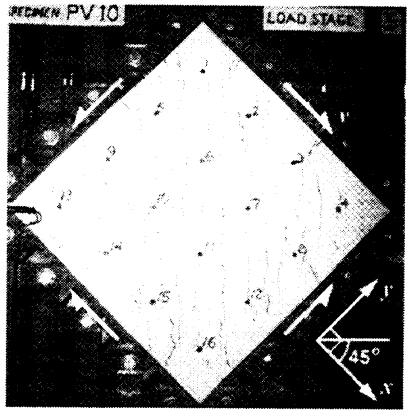

(a)

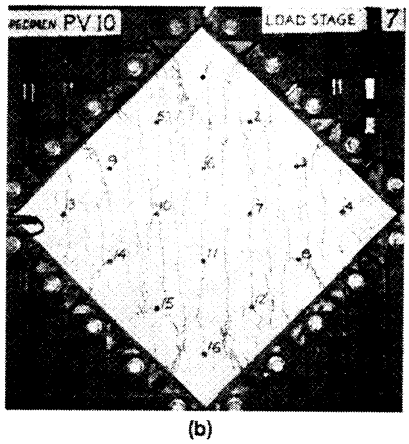

(b)

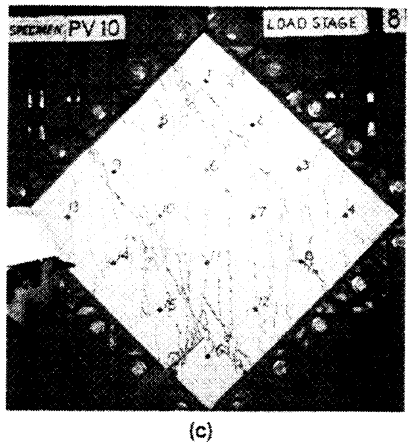

(c)

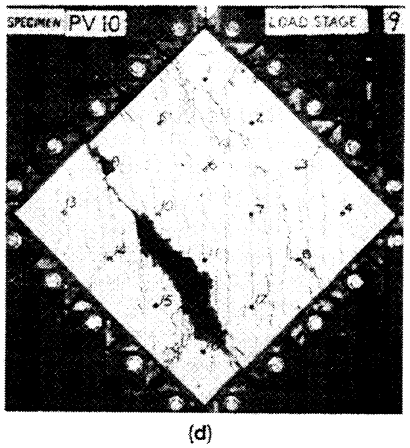

(d)

FIG. 1. Specimen PV10: (a) Prior to Yielding of Transverse Reinforcement; (b) at Ultimate Load Capacity; (c) Postpeak Condition; (d) Failure Condition

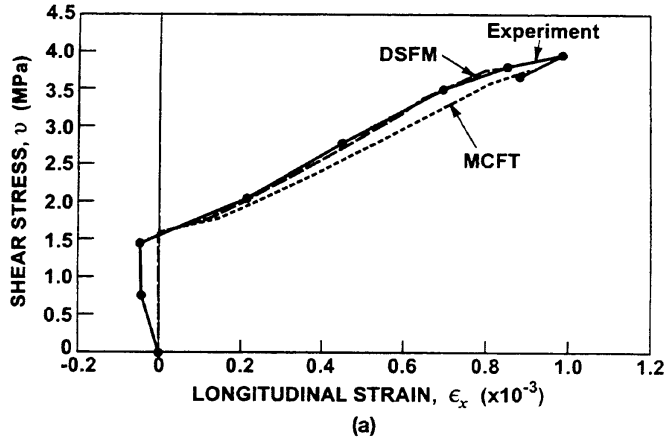

(a)

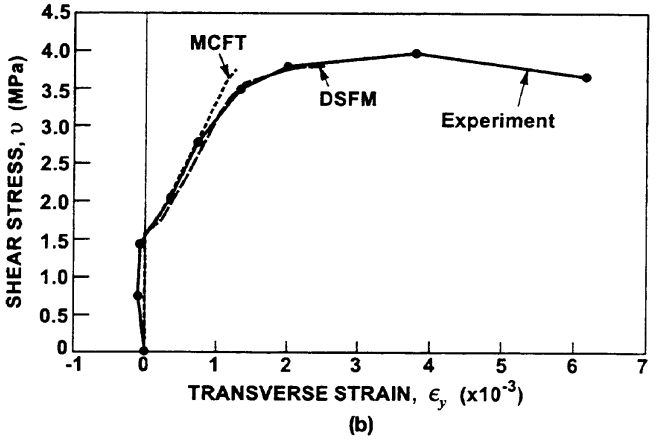

(b)

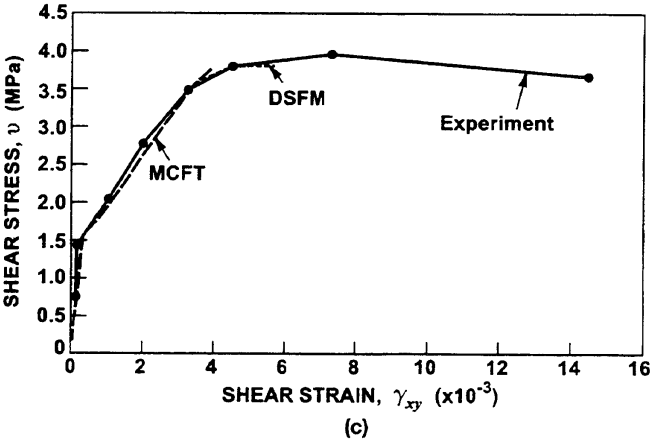

(c)

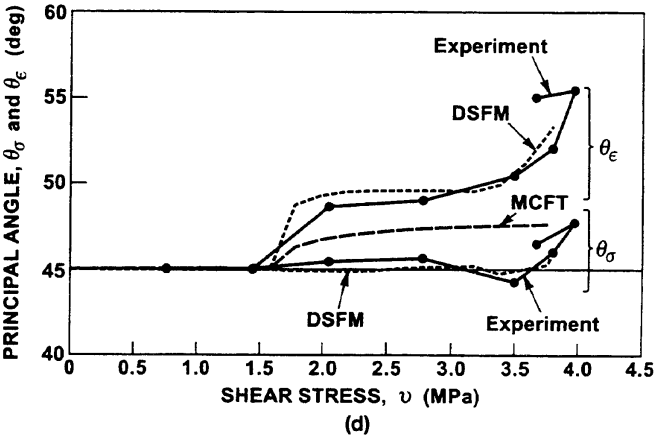

(d)

FIG. 2. Comparison of Load-Deformation Responses for PV10: (a) Longitudinal Reinforcement Strains; (b) Transverse Reinforcement Strains; (c) Shear Strain; (d) Inclination of Principal Stress and Apparent Principal Strain

of Panel PV10, and from the large number of other panels tested, include the following:

1. Where structural and loading conditions give rise to a reorientation of stress fields, the rotation of the stress field normally lags behind that of the strain field. This is contrary to the assumption made in full rotating-crack models, which typically enforce a coaxiality of stresses and strains.
2. While the rotation of the stress field is delayed somewhat, it eventually undergoes a gradual and progressive reorientation as existing cracks propagate and new cracks develop. This is contrary to the assumption typically made in fixed-crack models; that is, that crack angles largely remain fixed until, possibly, new cracks form at some alternate inclination.
3. The prevailing direction of the cracks in the concrete seems to correspond closely to the inclination of the calculated average principal stresses. Again, this is contrary to what is normally assumed in fixed-crack models.

The observations above are indicative of a crack slip component contributing to the total deformations occurring in the element. This was apparent in the test specimens from the observed localized ridging and crushing of concrete along crack surfaces, and from relative displacements measured across cracks. That the DSFM attempts to capture this aspect of behavior, while the MCFT does not, is significant. Shown in Fig. 2 are the responses predicted for Panel PV10 using the DSFM and MCFT formulations. The DSFM provides an accurate portrayal of the behavior of the element. While the MCFT provides an almost equally accurate calculation of the strength and load-deformation response of the element, it does not completely represent the observed crack and failure response. As will be shown later, the inclusion of rigid slip along the cracks is an important aspect in modeling the behavior of some reinforced concrete elements.

PANEL ELEMENTS

Three series of test panels were examined: the PV-, PB-, and PA-/PHS-Series specimens. The PV-Series panels, tested by Vecchio and Collins (1982), were the original panels on which the constitutive models of the MCFT were based. These panels were generally orthogonally reinforced and subjected to various conditions of shear and normal stresses. The PB-Series panels were tested by Bhide and Collins (1989); these were generally uniaxially reinforced and subjected to various combinations of uniaxial tension and shear. The PA- and PHS-Series panels were tested by Vecchio et al. (1994). This last set involved panels constructed from high strength concrete, orthogonally reinforced ($\rho_y < \rho_x$), and subjected to various combinations of shear and normal stress.

Analyses were performed for all panels using both the DSFM and the MCFT. The computed shear capacities, and comparisons to the experimentally determined strengths, are given in Fig. 3 for the 40 panels examined. The analytical model based on the DSFM, using the hybrid crack slip model previously described, produced a mean of 1.02 and a coefficient of variation (COV) of 9.6% for the ratio of theoretical to experimental shear strength. This is somewhat better than the estimates of capacity obtained from the MCFT, which produced a mean of 1.05 and a COV of 10.3%. In particular, the MCFT predictions for the PB-Series panels were consistently high; on average, overestimating the strength of these uniaxially reinforced elements by 14%. The accuracy of the DSFM calculations was generally equally good for all three series of panels, although the PB-Series panels showed more scatter. It should be noted, however, that several of the panels in this series failed at shear stresses at or marginally above the cracking load; hence, accuracy was significantly dependent on the estimate of the concrete tensile strength.

Panel	f_c' (MPa)	ρ_x (%)	ρ_x (%)	Loading $\sigma_x:\sigma_y:\upsilon$	$\upsilon_{u\text{-}exp}$ (MPa)	$\upsilon_{u\text{-}theor}/\upsilon_{u\text{-}exp}$ MCFT	DSFM
PV10	14.5	1.79	1.00	0:0:1	3.97	0.947	0.957
PV11	15.6	1.79	1.31	0:0:1	3.56	1.011	1.034
PV12	16.0	1.79	0.45	0:0:1	3.13	1.016	0.958
PV16	21.7	0.74	0.74	0:0:1	2.14	0.935	0.935
PV18	19.5	1.79	0.32	0:0:1	3.04	1.138	1.085
PV19	19.0	1.79	0.71	0:0:1	3.95	1.043	1.023
PV20	19.6	1.79	0.89	0:0:1	4.26	1.042	1.042
PV21	19.5	1.79	1.30	0:0:1	5.03	1.002	1.049
PV22	19.6	1.79	1.53	0:0:1	6.07	1.023	1.107
PV23	20.5	1.79	1.79	-0.39:-0.39:1	8.87	0.812	0.902
PV25	19.3	1.79	1.79	-0.69:-0.69:1	9.12	0.816	0.886
PV27	20.5	1.79	1.79	0:0:1	6.35	1.023	1.164
PV28	19.0	1.79	1.79	0.32:0.32:1	5.80	0.985	1.125
Vecchio and Collins Panels					Mean	0.984	1.021
					COV(%)	9.2	8.6
PA1	49.9	1.65	0.82	0:0:1	6.34	0.974	0.979
PA2	43.0	1.65	0.82	0:0:1	6.22	0.993	0.998
PHS1	72.2	3.23	0.00	0:0:1	2.95	1.035	0.976
PHS2	66.1	3.23	0.41	0:0:1	6.66	0.970	0.912
PHS3	58.4	3.23	0.82	0:0:1	8.19	1.109	1.103
PHS4	68.5	3.23	0.82	0.25:0.25:1	6.91	1.014	0.976
PHS5	52.1	3.23	0.41	0.25:0.25:1	4.81	0.910	0.855
PHS6	49.7	3.23	0.41	-0.25:-0.25:1	9.89	0.890	0.890
PHS7	53.6	3.23	0.82	-0.25:-0.25:1	10.30	1.105	1.152
PHS8	55.9	3.23	1.24	0:0:1	10.80	0.991	1.024
PHS9	56.0	3.23	0.41	-0.25:-0.25:1	9.37	1.009	0.998
PHS10	51.4	3.23	1.24	0.25:0.25:1	8.58	0.998	1.007
Aspiotis Panels					Mean	1.000	0.989
					COV(%)	6.5	8.4
PB6	17.6	1.09	0.00	1:0:1	1.15	1.176	1.086
PB8	20.4	1.09	0.00	2.98:0:-1	0.80	1.238	1.206
PB10	24.0	1.09	0.00	5.94:0:-1	0.56	1.200	1.193
PB14	41.1	2.02	0.00	3.01:0:-1	1.54	1.042	0.927
PB16	41.7	2.02	0.00	1.96:0:-1	1.42	1.197	1.176
PB17	41.6	2.02	0.00	5.93:0:-1	1.22	1.023	0.953
PB18	25.3	2.20	0.00	0:0:-1	1.72	1.221	1.221
PB19	20.0	2.20	0.00	1.01:0:-1	1.28	1.305	1.142
PB20	21.7	2.20	0.00	2.01:0:-1	1.42	1.085	0.953
PB21	21.8	2.20	0.00	3.08:0:-1	1.42	1.000	0.874
PB22	17.6	2.20	0.00	6.09:0:-1	1.03	1.080	0.972
PB29	41.6	2.02	0.00	2.02:0:-1	1.49	1.188	1.054
PB30	40.4	2.02	0.00	2.96:0:-1	1.48	1.088	0.961
PB31	43.4	2.02	0.00	5.78:0:-1	1.15	1.092	1.017
PB32	57.7	2.20	0.00	3.01:0:-1	1.49	1.114	1.023
Bhide Panels					Mean	1.136	1.051
					COV(%)	7.8	10.8
Total:					Mean	1.046	1.022
					COV(%)	10.3	9.6

FIG. 3. Results of Analyses of Panel Specimens

Load-deformation plots for the representative Panels PV23, PB20, PV20, and PHS8 are given in Fig. 4. Note that Panel PV23 was subjected to biaxial compression and shear and experienced only minor cracking prior to sustaining a crushing/shear failure of the concrete. Prior to failure, the panel experienced no yielding of the reinforcement nor rotation of the crack direction. Panel PB20, being uniaxially reinforced, experienced pronounced rotation of the crack directions before reaching ultimate capacity. Panels PV20 and PHS8 were biaxially reinforced, but due to the dissimilarities between reinforcement ratios, experienced pronounced shear slip on the cracks after yielding of the transverse reinforcement. It is suggested here that Panels PV23 and PB20 represent the two extremes in the range of structural conditions encountered in cracked reinforced concrete panel elements. Panels PV20 and

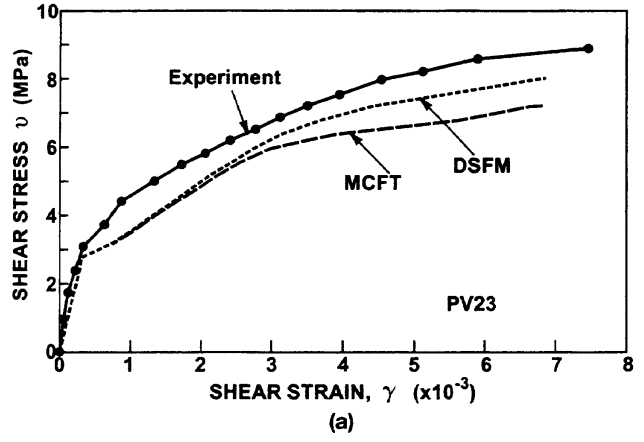

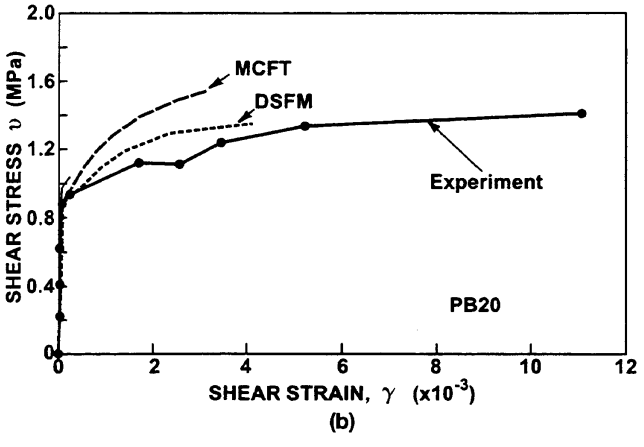

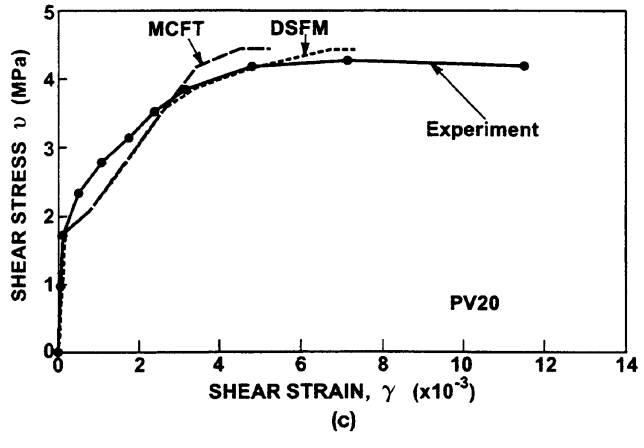

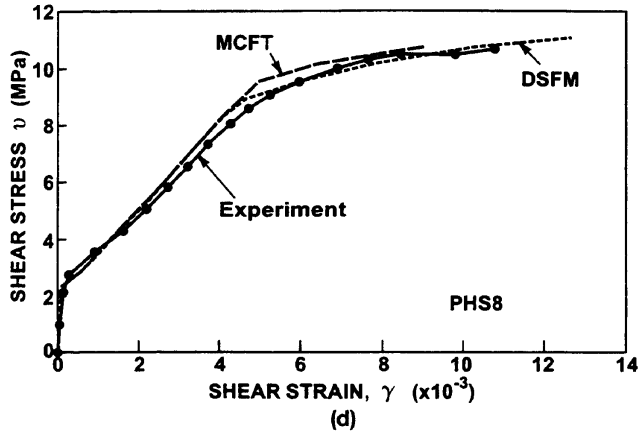

FIG. 4. Load-Deformation Plots for Representative Panels: (a) Panel PV23; (b) Panel PB20; (c) Panel PV20; (d) Panel PHS8

PHS8 represent the more typical panel element; the former with normal strength concrete and the latter with high strength concrete.

In Fig. 4, the responses ascribed to the DSFM are those determined using the hybrid crack slip model. In general, it can be noted that the load-deformation responses show reasonable agreement with the experimental values. The predicted strength and stiffness of Panel PV23 is lower than measured, but this appears to be somewhat related to an underestimate of the cracking stress. For Panel PB20, the postcracking stiffness, ductility and ultimate strength are all reasonably well represented. For both panels, the DSFM-derived responses are significantly improved over those obtained from the MCFT. The responses obtained for Panels PV20 and PHS8, showing excellent correlation, are more typical of the accurate correlation obtained for orthogonally reinforced elements in which one reinforcement component yields but the other does not. Here, all aspects of the response are well represented by the DSFM, as seen in Fig. 5 for Panel PV20. Note that, for these types of elements, the MCFT also provides excellent correlations.

SHEAR BEAMS

The MCFT has been shown to provide accurate simulations of the response of beams containing shear reinforcement of amounts equal to 0.2% or greater (Vecchio and Collins 1988). For such beams, the correlations obtained from DSFM analyses will be essentially similar. However, for beams containing little or no shear reinforcement, or for beams simultaneously subjected to axial compression (and hence experiencing minimal cracking), the results from MCFT have shown reduced accuracy (Vecchio 1999). Furthermore, as has been discussed, it is under such conditions that the results of the DSFM diverge from those of the MCFT. Hence, the corroboration studies presented here concentrate on these beam types.

Three series of beams were considered. First, the set of 12 beams tested by Bresler and Scordelis (1963), often used as a benchmark, were modeled because they cover a representative range of conditions in terms of reinforcement amounts, shear spans, and failure modes. The second set modeled involved 18 beams tested by Stanik and Collins (1998). This set is particularly challenging in terms of analytical modeling for the following reasons: (1) the beams were large-scale, with the majority being 1,000 mm deep, raising the prospect of size effects; (2) the beams had a relatively short shear span ratio —a condition where reorientation of crack direction can significantly alter the load-resisting mechanisms; (3) the majority of the beams contained no shear reinforcement; and (4) several of the beams were constructed using high strength concrete. With respect to the latter condition, Stanik and Collins have noted that the strength of shear-critical high strength concrete beams is significantly lower than what current codes predict. The third series of specimens considered involves a series of strip beams, subjected to various combinations of axial compression and transverse shear, tested by Gupta (1998). This series will test the analytical procedures under conditions where cracking is minimal and where capacity is governed by the formation of a single dominant crack.

The beams were modeled for finite-element analysis taking advantage of symmetry to model half spans. With the Bresler and Scordelis beams, a mesh of 32 × 9 constant strain (eight degrees of freedom) rectangular elements were used for the 7.32-m-span beams; 39 × 9 elements for the 9.14-m-span beams; and 40 × 9 elements for the 12.8-m-span beams. The Stanik beams were modeled with a 40 × 12 element mesh, and the Gupta beams utilized an 18 × 10 element mesh. All material properties used were as given in the respective references except that the concrete cracking stress was approxi-

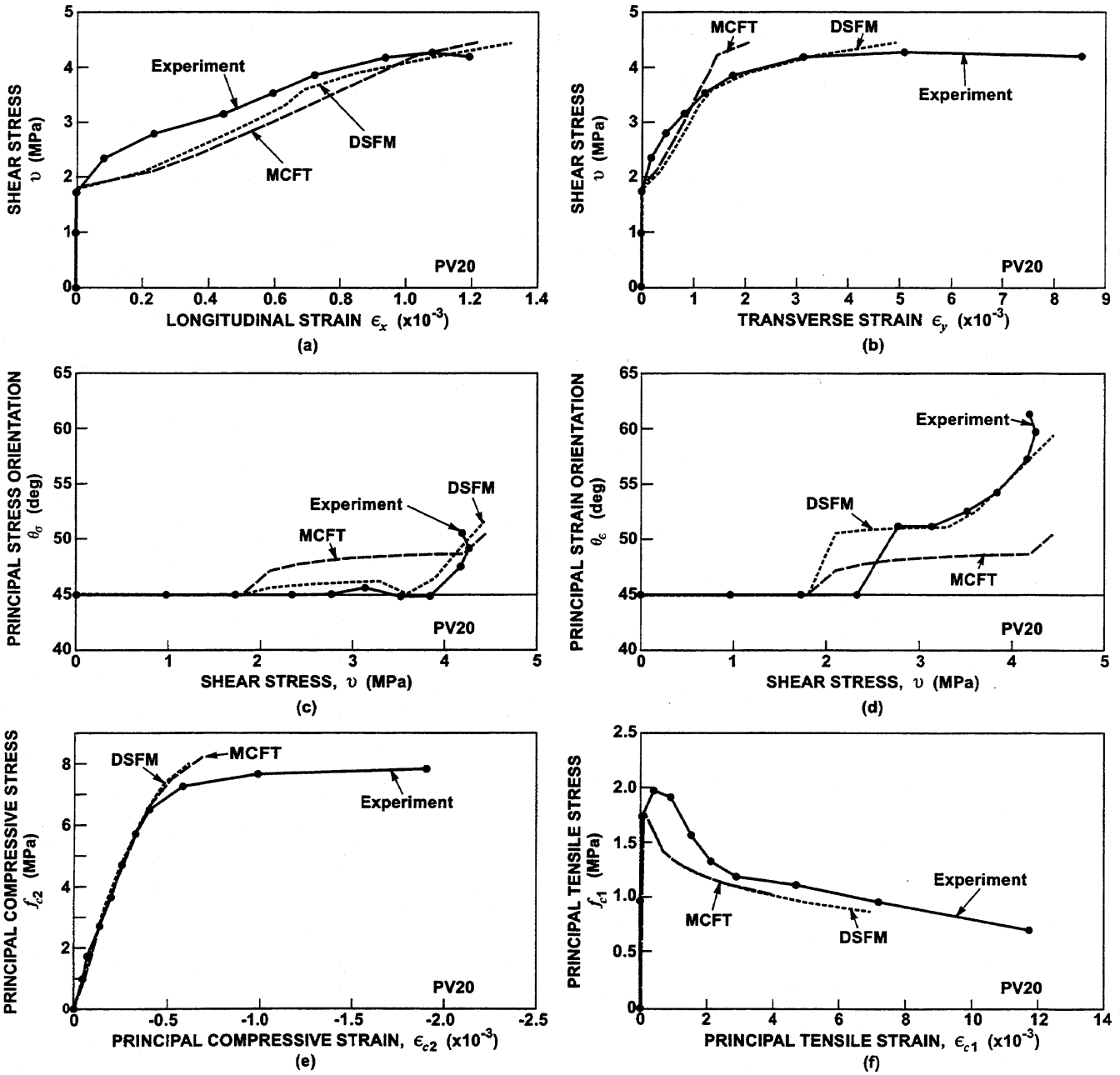

FIG. 5. Observed and Calculated Responses for Panel PV20: (a) Longitudinal Reinforcement Strains; (b) Transverse Reinforcement Strains; (c) Inclination of Principal Stresses; (d) Inclination of Principal Strains; (e) Principal Compressive Stress in Concrete; (f) Principal Tensile Stress in Concrete

mated using $0.65(f'_c)^{0.33}$. The Bresler-Scordelis beams and the Gupta beams were subjected to force-controlled loading, with shear load increments of 2.5 and 5.0 kN, respectively. The Stanik beams were subjected to displacement-controlled loading, with midspan displacement increments of 0.25 mm imposed.

The behavior of the Bresler-Scordelis beams was modeled reasonably well, although the tendency was to underestimate the load capacity (Fig. 6). This tendency was likely due to two factors. First, for the beams containing no shear reinforcement (OA1, OA2, and OA3), the computed shear capacity of the beams was highly dependent on the concrete cracking stress. The values used were lower-bound estimates and were significantly less than the moduli of rupture reported by Bresler and Scordelis. Second, many of the remaining beams were overreinforced in flexure and ultimately sustained crushing on the compression face but, in some cases (e.g., A2), were able to achieve capacities well above the theoretical pure flexure strength. In the analyses of these beams, numerical difficulties were encountered due to crushing of concrete in the vicinity of the top loading plate, resulting in reduced theoretical load capacities. Nevertheless, the typical load-deformation responses shown in Fig. 7 indicate good correlation between the experimental behavior and that calculated using the DSFM. The computed responses obtained using the MCFT, also shown in Fig. 7, provide equally good correlation for this representative set of beams.

The computed responses for the Stanik beams showed more scatter, owing to the uncommon characteristics of the test specimens as previously discussed. From Figs. 6 and 8, it can be seen that, while both the DSFM and MCFT had the tendency to overestimate strengths, the accuracy was somewhat improved with the DSFM. However, what is perhaps more significant is the better representation of the failure mechanism. With the DSFM, there is a reduced ability for the concrete compression struts to reorient themselves such as to pro-

Beam	$V_{u\text{-}exp}$ (kN)	$V_{u\text{-}theor}$ (kN)			$V_{u\text{-}theor}/V_{u\text{-}exp}$		
		DSFM	MCFT	ACI	DSFM	MCFT	ACI
BM100	343	346.7	389.4	424.3	1.011	1.135	1.237
BM100D	462	431.6	466.5	424.3	0.934	1.010	0.918
BN100	192	175.8	191.1	281.9	0.916	0.995	1.468
BN100D	258	275.4	312.3	281.9	1.067	1.210	1.093
UM100	750	759.2	759.0	413.9	1.012	1.012	0.552
UM100D	910	835.4	892.6	413.9	0.918	0.981	0.455
UN100	593	784.6	825.2	302.2	1.323	1.392	0.510
UN100D	637	774.2	829.4	302.2	1.215	1.302	0.474
WM100C	699	585.3	769.6	1177.0	0.837	1.101	1.684
WM100D	834	837.1	968.7	1142.0	1.004	1.162	1.369
BRL100	164	199.6	204.5	382.9	1.217	1.247	2.335
BRH100	357	217.6	366.5	382.9	0.610	1.027	1.073
BH100	193	279.5	250.3	382.9	1.448	1.297	1.984
BH100D	281	355.9	424.1	382.9	1.267	1.509	1.363
BH50	132	114.9	132.6	186.3	0.870	1.005	1.411
BH50D	193	175.0	194.9	186.3	0.907	1.010	0.965
BN50	132	92.6	104.7	136.8	0.702	0.793	1.036
BN50D	163	138.1	150.0	136.8	0.847	0.920	0.839
Stanik Beams				Mean	1.006	1.117	1.154
				COV(%)	21.7	16.2	44.9
OA1	166.5	147.2	161.7	112.6	0.884	0.971	0.676
OA2	178.0	130.3	143.8	114.9	0.732	0.808	0.645
OA3	189.0	111.4	127.3	144.4	0.589	0.674	0.764
A1	233.5	244.1	240.5	163.4	1.045	1.030	0.700
A2	244.5	201.7	205.3	162.2	0.825	0.840	0.663
A3	233.5	179.7	191.0	187.5	0.770	0.818	0.803
B1	222.0	222.7	216.3	138.8	1.003	0.974	0.625
B2	200.0	167.0	171.9	136.4	0.835	0.860	0.682
B3	178.0	164.1	183.2	159.6	0.922	1.029	0.896
C1	155.5	167.9	164.8	111.3	1.080	1.060	0.716
C2	162.0	132.0	137.6	103.8	0.815	0.849	0.641
C3	135.5	134.8	142.6	115.8	0.995	1.052	0.855
Bresler and Scordelis Beams				Mean	0.875	0.914	0.722
				COV(%)	16.3	13.4	12.2
PC1	437	490	595	359	1.121	1.362	0.822
PC2	863	860	850	1346	0.997	0.985	1.560
PC3	845	685	760	1165	0.811	0.899	1.379
PC4	401	390	485	273	0.973	1.209	0.681
PC5	679	945	930	1889	1.392	1.370	2.782
PC6	668	715	755	1094	1.070	1.130	1.638
PC7	387	355	400	233	0.917	1.034	0.602
PC8	497	630	610	760	1.268	1.227	1.529
PC9	516	610	610	540*	1.182	1.182	1.047
PC10	726	1020	985	1277	1.405	1.357	1.759
PC11	754	1040	1040	900*	1.379	1.379	1.194
PC12	490	375	450	262	0.765	0.918	0.535
PC13	680	645	700	982	0.949	1.029	1.444
PC14	686	780	735	700*	1.137	1.071	1.020
PC15	358	385	385	350*	1.075	1.075	0.978
PC16	945	925	930	900*	0.979	0.984	0.952
PC17	707	735	735	660*	1.040	1.040	0.934
PC18	832	760	780	894	0.913	0.938	1.075
PC19	751	770	775	680*	1.025	1.032	0.905
PC20	715	1010	1030	1544	1.413	1.441	2.159
PC21	767	755	810	1116	0.984	1.056	1.455
PC22	443	390	430	252	0.880	0.971	0.569
PC23	603	550	590	751	0.912	0.978	1.245
PC24	528	425	500	277	0.805	0.947	0.525
Gupta Beams				Mean	1.058	1.109	1.199
				COV(%)	18.4	15.0	45.1
Total:				Mean	1.000	1.068	1.078
				COV(%)	20.3	16.9	46.6

* Governed by flexural capacity

FIG. 6. Results of Analyses of Beam Specimens

vide a direct load path to the support. Hence, the failure mode is one dominated more by transverse shear displacements, resulting from the formation of a single dominant shear crack and rigid body slip along this crack. With the MCFT, there is a greater tendency for a splitting crack to form above the bottom longitudinal reinforcement and for a sliding shear failure

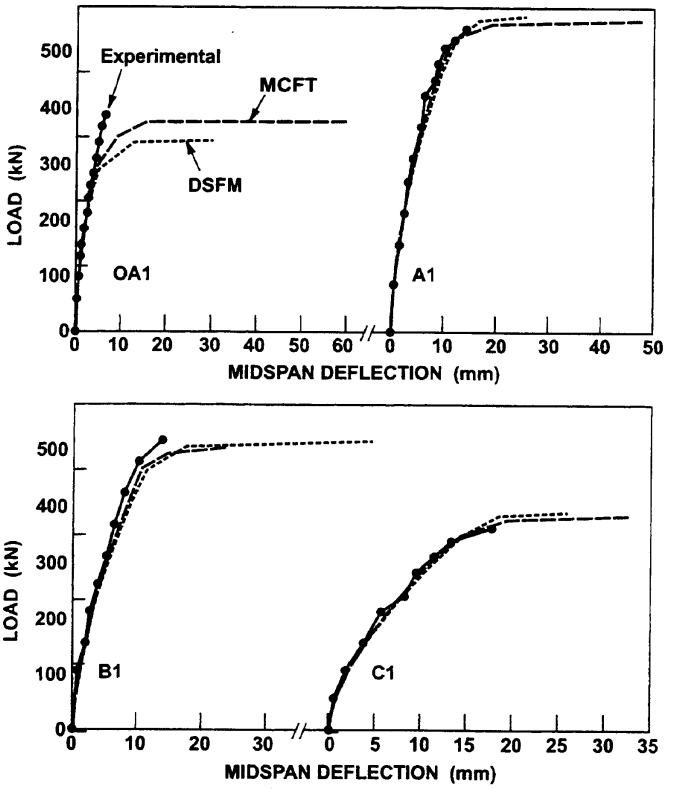

FIG. 7. Comparisons of Load-Deformation Responses for Typical Bresler-Scordelis Beams

to occur along this crack. These subtle differences are apparent in the displaced shapes for Beam WM100D shown in Fig. 9.

The behavior of the Gupta beams was typically dominated by the formation of a principal crack, with failure ensuing shortly thereafter. With increasing ratios of compression to shear, behavior became more brittle and somewhat more dependent on the ability of cracks to realign and form direct struts. The DSFM, in better modeling the delayed rotation of the cracks, resulted in improved predictions of strength. Direct measurements of the beam deflections were not obtained because of the test setup used; hence, comparisons of predicted and observed load-deformation responses were not possible. However, the ability of the DSFM to represent rebar strains and concrete surface strains was found to be reasonably good at all stages of loading.

For the three sets of beams combined, the ratio of calculated to observed shear capacity obtained using the DSFM has a mean of 1.00 and a COV of 20.3%. This is an improvement to the mean of 1.07 and COV of 16.9% obtained using the MCFT and significantly better than the 1.08 and 46.6% obtained using the American Concrete Institute (ACI) code formulations.

SHEAR WALLS

To gauge the accuracy of the analysis model under more common conditions, two series of shear walls tested by Lefas et al. (1990) were studied. The test program consisted of 13 large-scale walls tested under various conditions of axial and lateral load. The wall geometries were of two types: the Type I walls were relatively squat with a height-to-width ratio of 1.0; and the Type II walls were more slender with a height-to-width ratio of 2.0. In both cases, the walls were of rectangular cross section but contained a more heavily reinforced concealed column in the edge (flange) regions. The web regions of the walls were generally reinforced in the vertical and horizontal directions in accordance with ACI 318 specifications.

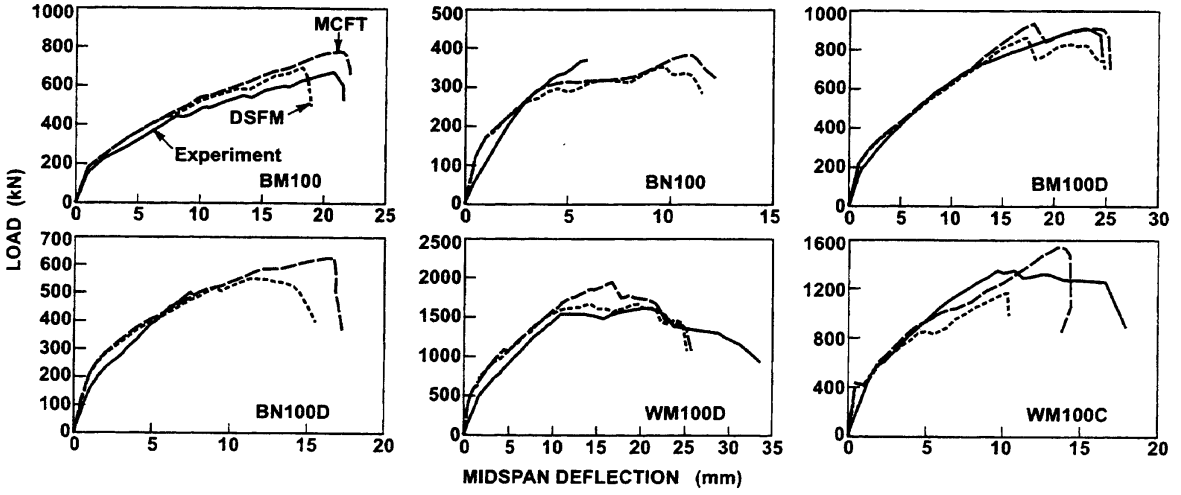

FIG. 8. Comparisons of Load-Deformation Responses for Typical Stanik Beams

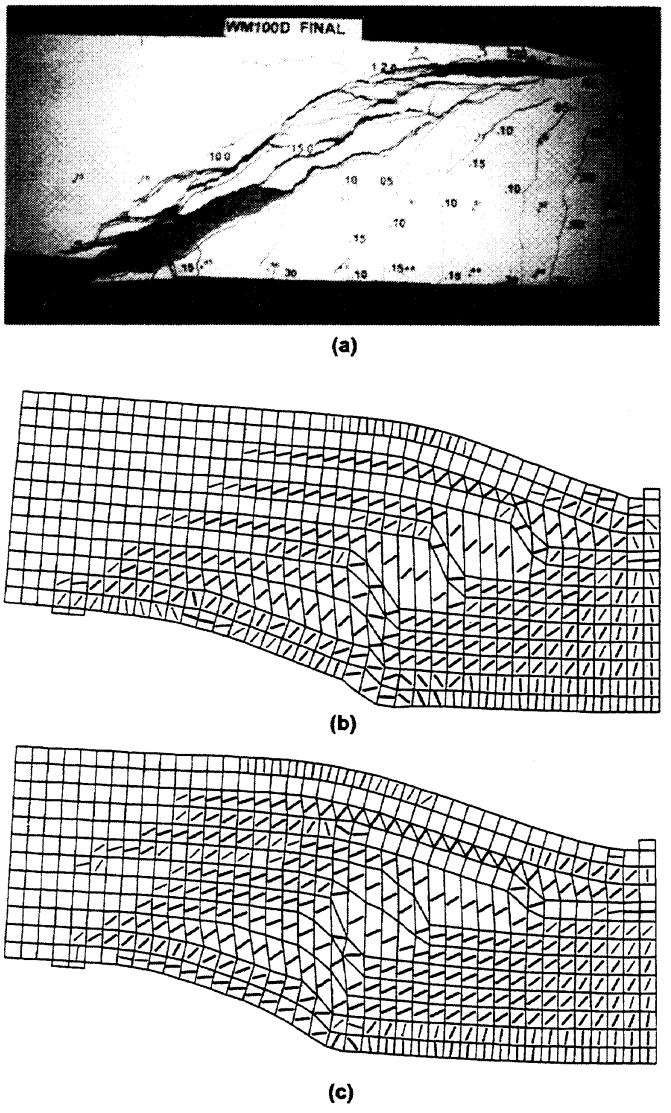

FIG. 9. Failure Mode of Stanik Beam WM100D; (a) from Experiment; (b) from DSFM Analysis; (c) from MCFT Analysis

The walls were subjected to constant axial loads combined with montonically increasing lateral load applied through the top spreader beam. They exhibited a strong ductile behavior, developing strengths greater than expected. Lefas et al. reported the development of triaxial compressive stress conditions at the base of the walls and in the concealed columns

Wall	$F_{u\,exp}$ (kN)	MCFT $F_{u\,theor}$ (kN)	MCFT $\frac{F_{u\,theor}}{F_{u\,exp}}$	DSFM $F_{u\,theor}$ (kN)	DSFM $\frac{F_{u\,theor}}{F_{u\,exp}}$
SW11	260	279	1.072	281	1.081
SW12	340	334	0.981	341	1.004
SW13	330	311	0.943	317	0.960
SW14	265	262	0.990	270	0.981
SW15	320	296	0.923	303	1.019
SW16	355	367	1.035	372	1.047
SW17	247	253	1.024	255	1.033
SW21	127	124	0.973	124	0.978
SW22	150	154	1.024	154	1.024
SW23	180	173	0.962	174	0.964
SW24	120	125	1.039	126	1.049
SW25	150	168	1.120	168	1.118
SW26	123	113	0.922	118	0.960
Mean			0.997		1.011
COV (%)			5.7		5.3

FIG. 10. Results of Analyses of Shear Wall Specimens

and attributed the high shear resistance of the walls to this condition.

Finite-element analyses were undertaken for the two series of walls tested. A 340-element mesh was used to represent the Type I walls, and a 536-element mesh was used for the Type II walls. The axial load was represented by constant-value nodal forces applied to the top spreader beam; the lateral loading was applied in the form of imposed horizontal displacement of the spreader beam. Note that no attempt was made to model base rotation due to rebar slip.

The analysis results are given in Fig. 10 for both the DSFM and MCFT analyses. Given in Fig. 11 are representative observed and computed load-deformation plots (for each wall type, one pair with no axial load, SW11 and SW21, and one pair with the highest level of axial load, SW16 and SW23). The strengths of the walls were computed accurately and with a low degree of scatter; the ratio of the calculated to observed strength for the 13 walls had a mean of 1.01 and a COV of 5.3%. The computed failure modes involved crushing of concrete in the compression toe region coupled with a sliding shear failure along the base in some cases; this corresponded well with the observed failures reported by Lefas et al. The computed deflections and ultimate ductility showed some variance relative to the observed responses but generally were accurately represented as well. Also notable is that there was virtually no difference between the results obtained from the DSFM and those obtained from the MCFT. In most situations involving orthogonally reinforced structures containing above-minimum levels of reinforcement, such is likely to be the case.

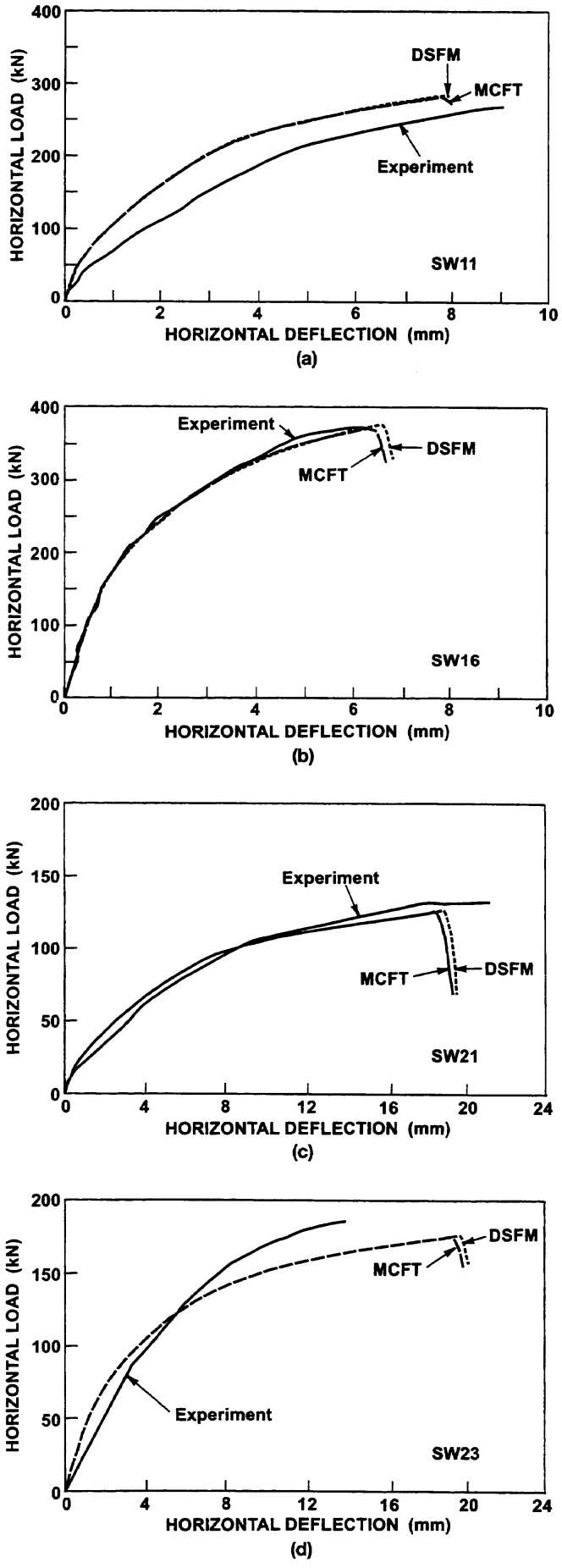

FIG. 11. Comparison of Load-Deformation Responses for Typical Lefas et al. Shear Walls

DISCUSSION AND FUTURE WORK

The DSFM appears to provide reasonably accurate simulations of response over a wide range of conditions and represents an improvement on the MCFT in terms of both accuracy and theoretical rigor. However, there are aspects of the formulation in need of further study.

First, the crack shear slip modeling warrants further attention. In the stress-based approach, an improved formulation may better account for the influence of initial slip and for possibly increased degrees of slip in high strength concrete. In the rotation-lag approach, a more rigorous relationship quantifying the lag-angle would be desirable, particularly if the analysis approach is to be extended to situations involving reversed cyclic loading.

The accuracy of the DSFM appears to deteriorate in beams containing heavy amounts of longitudinal reinforcement, no transverse reinforcement and subjected to a high shear-span-ratio loading conditions (e.g., Bresler-Scordelis Beams OA2 and OA3). It is not known whether this is due to a deficiency in the constitutive model, due to a deficiency in the finite-element modeling, or a consequence of the estimated cracking strengths of the concrete being so much lower than the moduli of rupture reported for this particular series of beams. Further study is required. With such beams, it was shown by Vecchio (1999) that using a concrete postcracking residual tensile stress of $0.10f'_c$ leads to significantly improved results. However, relying on such an empirical "concrete contribution" factor detracts from the transparency and rigor of the theory. Again, further study is required before the use of a residual tension term can be advocated.

CONCLUSIONS

The DSFM is shown to be a viable alternative model for the analysis of reinforced concrete elements. It is an extension of the MCFT, with the principal difference being that the DSFM explicitly includes rigid slip along crack surfaces into the compatibility relations for the element. This allows for a divergence of the angles of inclination of average principal stress and apparent average principal strain in the concrete. It also removes the need for an awkward crack slip check that currently complicates the MCFT. The model represents cracks as gradually rotating, but typically lagging behind the reorientation of the principal strains. As such, the DSFM combines aspects of both rotating-crack and fixed-crack models but is distinctly different from both in various key aspects. In comparing the predictions of the theory to experimental observations, the DSFM is seen to be more phenomenologically correct in its representation of reinforced concrete behavior than the MCFT, or other rotating-crack or fixed-crack models in general.

The accuracy of the proposed formulation was tested by examining correlations with the test results from panels, beams, and shear walls. It should be noted that most of the test specimens considered were difficult cases due to the nature of the reinforcement, cross section, or loading details. The DSFM was generally found to provide accurate calculations of strength, load-deformation response, and failure mode. However, with panels that were uniaxially reinforced, or with beams containing no shear reinforcement, the scatter of results was significant. Here, strength and behavior was highly dependent on the concrete cracking strength, which itself is subject to high variability. Hence, a consistently close correlation should not be expected with such elements, regardless of the analytical procedure being used. Nevertheless, the DSFM provided improved results compared to those obtained from the MCFT.

The corroboration studies also reaffirmed the strength of the

MCFT as a simple model providing good accuracy over a wide range of conditions. Although the MCFT's assumption of coaxiality of stresses and strains is shown to have some fault, as was known from the outset, its influence on predicted behavior is minor in most cases.

APPENDIX. REFERENCES

Bhide, S. B., and Collins, M. P. (1989). "Influence of axial tension on the shear capacity of reinforced concrete members." *ACI Struct. J.*, 86(5), 570–581.

Bresler, B., and Scordelis, A. C. (1963). "Shear strength of reinforced concrete beams." *ACI J.*, 60(1), 51–74.

Gupta, P. R. (1998). "Shear design of reinforced concrete members under axial compression." PhD thesis, Dept. of Civ. Engrg., University of Toronto, Toronto.

Lefas, I. D., Kotsovos, M. D., and Ambraseys, N. N. (1990). "Behaviour of reinforced concrete structural walls: Strength, deformation characteristics, and failure mechanism." *ACI Struct. J.*, 87(1), 23–31.

Okamura, H., and Maekawa, K. (1991). *Nonlinear analysis and constitutive models of reinforced concrete*, University of Tokyo.

Stanik, B. (1998). "The influence of concrete strength, distribution of longitudinal reinforcement, amount of transverse reinforcement and member size on shear strength of reinforced concrete members." MASc. thesis, Dept. of Civ. Engrg., University of Toronto, Toronto.

Vecchio, F. J. (1999). "Analysis of shear-critical reinforced concrete beams." *ACI Struct. J.*, 97(1), 102–110.

Vecchio, F. J. (2000). "Disturbed stress field model for reinforced concrete: Formulation." *J. Struct. Engrg.*, ASCE, 126(9), 1070–1077.

Vecchio, F. J. (2001). "Disturbed stress field model for reinforced concrete: Implementation." *J. Struct. Engrg.*, ASCE, 127(1), 12–20.

Vecchio, F. J., and Collins, M. P. (1982). "Response of reinforced concrete to in-plane shear and normal stresses." *Rep. No. 82-03*, Dept. of Civ. Engrg., University of Toronto, Toronto.

Vecchio, F. J., and Collins, M. P. (1986). "The modified compression field theory for reinforced concrete elements subjected to shear." *ACI J.*, 83(2), 219–231.

Vecchio, F. J., and Collins, M. P. (1988). "Predicting the response of reinforced concrete beams subjected to shear using the MCFT." *ACI Struct. J.*, 85(3), 258–268.

Vecchio, F. J., Collins, M. P., and Aspiotos, J. (1994). "High-strength concrete elements subjected to shear." *ACI Struct. J.*, 91(4), 423–433.

Walraven, J. C. (1981). "Fundamental analysis of aggregate interlock." *J. Struct. Engrg.*, ASCE, 107(11), 2245–2270.